Desalination and Water Treatment
www.deswater.com
doi: 10.5004/dwt.2022.28902

276 (2022) 237–249
November

Pathways, by-products, reaction intermediates, and kinetics study of degradation of profenofos via photo-assisted peroxidation

Railson O. Ramos[a], Maria V.C. Albuquerque[a], Suelly F. da Silva[a,b], Wellington S. Lyra[b], Mário César U. Araújo[b], José T. de Sousa[a], Valderi D. Leite[a], Wilton S. Lopes[a,*]

[a]*Departamento de Engenharia Sanitária e Ambiental,Universidade Estadual da Paraíba, Rua Baraúnas, 351, Bairro Universitário, Zip Code: 58429-500, Campina Grande, PB, Brazil, emails: wiltonuepb@gmail.com (W.S. Lopes), railson_uepb@outlook.com (R.O. Ramos), virginia.albuquerque@yahoo.com.br (M.V.C. Albuquerque), susuellyfernandes@hotmail.com (S.F. da Silva), tavaresuepb@gmail.com (J.T. de Sousa), mangabeiraleite@gmail.com (V.D. Leite)*
[b]*Departamento de Química,Universidade Federal da Paraíba, Curva da Sucupira, s/n, Caixa Postal 5093, Zip Code: 58051-970, João Pessoa, PB, Brazil, emails: wellington@ccen.ufpb.br (W.S. Lyra), mariougulino@gmail.com (M.C.U. Araújo)*

Received 28 December 2021; Accepted 5 August 2022

ABSTRACT

This article presents, in detail, the paths and mechanisms, main by-products, and a kinetic study of the oxidation of profenofos (PFF) by $HO^{\bullet}$ radicals. Photo-assisted peroxidation was the precursor reaction for generation of radicals; the effect of UV-C (245 nm) radiation was evaluated. The results of the kinetics study indicated that the best fit for the experimental data was the pseudo-first-order model; further, that oxidation occurs in a fast initial stage and a slow final stage. In an acidic environment, the fast oxidation stage was favored over the slow stage; while in the basic medium the opposite behavior was observed. Eight oxidation by-products and 29 reaction intermediates were identified. The main mechanisms involved in the mineralization of PFF were reactions of electron abstraction, $HO^{\bullet}$ abstraction, $H^{\bullet}$ abstraction, substitution, displacement, and addition of electrons. The rapid oxidation step was related to the mining of the O–C_2H_5 and S–C_3H_7 chains of the intermediate *O*-ethyl *S*-propyl phosphonothioate. The slow oxidation step included the mineralization of 4-bromo-2-chlorophenyl and derivatives.

Keywords: Profenofos; Photo-assisted peroxidation; Kinetics study; Degradation pathways; By-products identification

1. Introduction

Studies on the degradation of organophosphate pesticides have increased due to environmental contamination caused by these pollutants which are widely used in agriculture [1,2]. *O*-(4-bromo-2-chlorophenyl) *O*-ethyl *S*-propyl phosphorothioate is the systematic name of profenofos (PFF), one of the most widely used insecticides over the last two decades to control lepidopteron pests of cotton and tobacco, and on vegetables such as corn, potatoes, soybeans and sugar beets [3,4]. PFF is a well-known chiral organophosphate that could cause enantioselective cytotoxicity, DNA damage in PC_{12} cells and acetylcholinesterase inhibition, as described in previous studies [5,6]. For remediation of environmental contamination by organophosphates, the most studied treatment is with advanced oxidative processes (AOPs) [7,8]. The great advantage of AOPs is the ability to convert organic matter to minerals, carbon dioxide, and water. However, this conversion is often incomplete for complex molecules and some by-products with characteristic structures of organophosphates can be formed during the oxidations, even under optimized conditions [9,10]. Given this, in-depth studies on oxidation pathways and by-products are indispensable from an environmental and health point of view.

* Corresponding author.

The degradation of PFF through AOPs such as heterogeneous photocatalysis (TiO_2/UV-C) [11], Fenton (Fe^{2+}/H_2O_2) [12] and direct photodegradation (UV-C) [13] have already been reported in the literature. Results of kinetics studies, degradation pathways, and identification of by-products generated in these three ways of degradation have successfully been presented. Among AOPs, one that stands out for its simplicity of application, low cost and efficiency is photo-assisted peroxidation (H_2O_2/UV-C) [14,15] as well as having the facility to generate hydroxyl radicals [16]. This AOP has already been reported for the degradation of PFF by the study of Amin et al. [17] and Badawy et al. [18], but the researchers did not report its degradation pathways or by-products. Since by-products can have higher toxicity and/or are often more persistent and mobile than the precursor substance [19,20], this kind of information would be relevant for remediation of contaminated environments. Moreover, by-products in the environment can play a significant role in defining the impact of pesticides on both human health and natural ecosystems [21,22].

In this work, a photocatalytic reactor, total organic carbon (TOC), ultra-high performance liquid chromatograph-mass spectrometry (UHPLC-MS), and direct infusion mass spectrometry (DIMS) analyzers were used to perform a kinetic study and investigate in detail the degradation pathways of PFF by photo assisted peroxidation, to correlate kinetic parameters with molecular oxidation routes, and to identify the main by-products, mechanisms, secondary rations, and reaction intermediates.

2. Experimental

2.1. Reagents, solutions, and sample

All chemicals used in this work were analytical grade; ultrapure water (Milli-Q Millipore system) was used throughout the work. PFF, methanol, acetonitrile, and titanium (IV) bis (ammonium lactate) dihydroxide solution were purchased from Sigma-Aldrich (St. Louis, MO, USA). Sodium hydroxide, hydrochloric acid, sulfuric acid, and hydrogen peroxide were purchased from Vetec (São Paulo, SP, BR).

A stock solution of 2.5 mg/mL of PFF was prepared in a 1:1 acetonitrile/ultrapure water mixture. All working solutions were prepared by suitable dilution of the stock solution in the same mixture of solvents.

2.2. Apparatus

degradation experiments were carried out in a 3.2 L tubular plug flow reactor equipped with a 15 W mercury vapor UV-C (254 nm) lamp with a surface irradiance of 22 mW/cm^2 (1.5 J/s·L) (Fig. S1). A quartz tube (SUNSUN, JUP-21) was used to cover the lamp. A glass capacitor (Pyrex, 2560) as a heat exchanger was used to maintain temperature at approximately 25°C. The recirculation of the PFF solution was performed by using a micro diaphragm pump (JRK, 555SH) operating at a flow-rate of 13 L/min. The recirculation line was coupled to an equalization tank in which detectors for pH, redox potential, and temperature were placed. The addition of reagents and sampling was carried out through the equalization tank by valves.

2.3. Analytical procedures

The analysis, methods, and instruments used in this work are presented in Supplementary Table S1. Standard electrodes for temperature, pH, and redox potential were inserted into the equalization talk and maintained under continuous stirring. Their measurements were taken after the stabilization of each analytical response. To avoid errors in pH measurements due to the production of CO_2 and oxygenation, the recirculation line was sealed.

Quantitative analysis of PFF was carried out in a UHPLC 3000 coupled to a LCQ Fleet Mass Spectrometer (Thermo Scientific, Waltham, MA, USA). The reverse-phase chromatographic column was a C18, 100 mm × 2.1 mm, 3 μm and the mobile phase was methanol/acetonitrile (1:1, 3 mL/min) in the isocratic elution mode. The temperatures of the column and sampler were 40°C and 25°C, respectively. The m/z = 375 in the electron impact ionization mode (ESI^+) was used for obtaining the analytical response (peak area). Spray voltage was set at 5 kV and the spray was stabilized with a nitrogen flow. The temperatures of vaporizer and transfer capillaries were 378°C and 200°C, respectively. A volume of 10 μL was used for the injection of standard solutions and samples. The analytical curve comprised standard solutions in a range of 25–1,000 μg/L at seven levels of concentration. Before analysis, standard solutions and samples were acidified with 0.6 M/L HCl solution up to pH = 3.0.

Before the investigation of by-products by DIMS, the solid-phase microextraction (SPME) technique employing C18 columns (500 mg/6 mL, Vertical Co., Ltd.) coupled to a vacuum manifold (TR-004012, Teknokroma) was used. The filtration of the samples was performed at 1 mL/min flow rate. Thereafter the sample was re-dissolved in methanol. The mass spectra were recorded under the same conditions described for UHPLC-MS, but a volume of 100 μL was used for each injection. Data were analyzed with the Xcalibur software (Thermo Scientific, Waltham, MA, USA).

Total organic carbon (TOC) analyses were carried in a TOC analyzer (Multi N/C® 3100 analyzer, Analytik Jena, Germany) equipped with an automated sampler with and chemical detection system by moist medium and UV. Before analysis, 5 mL of the sample was dispersed into 15 mL of ultrapure water and acidified by the addition of 500 μL of concentrated H_2SO_4.

Residual H_2O_2 was determined spectrophotometrically by the method in which titanium (IV) bis(ammonium lactate) dihydroxide reacts with hydrogen peroxide in aqueous medium to produce a titanic complex that absorbs at 410 nm [23]. The analytical curve comprised standard solutions in the range of 1.25–50 mg/L at six concentration levels. 300 μL of titanium(IV) bis(ammonium lactate) dihydroxide solution and 3 mL of the standard solutions/sample were homogenized in a vortex. After 5 min in the absence of light, absorbance measurements were performed.

2.4. Procedures for degradation, kinetics and of by-products studies

An initial assay was carried out to evaluate the efficiency of the H_2O_2/UV-C system in the oxidation of the organic matter Crittenden et al. [25] and Azizi et al. [28]. The pH of a

50 mg/L PFF standard solution was adjusted by the addition of 0.5 mM/L NaOH up to 8.0. For the initial oxidation of PFF, the H_2O_2 concentration was a 3.125 mM/L (0.0625 mM/L off H_2O_2 for each 1 mg/L PFF). At each defined period (0, 1, 2.5, 5, 15, 30, 45, and 60 min) an aliquot of 5 mL was taken and analyzed by TOC according to the previous section.

For the definitive degradation, kinetics and by-products studies were carried out by using a 1.05 mg/L PFF (or 1,050 μg/L) standard solution under six different experimental conditions (ECs) as described in supplementary Table S1, with concentrations ranging from 0.25 to 0.5 mM/L and a pH range from 2 to 8. At the same periods as in the preliminary degradation study, an aliquot of 5 mL was also taken and analyzed by UHPLC and DIMS according to the previous section.

3. Results and discussion

3.1. Preliminary degradation study

An estimate of the maximum oxidative capacity of the H_2O_2/UV-C system over the PFF molecule can be made from the results of TOC analysis. As the reaction goes on, the TOC values decrease, according to Fig. 1A. An efficiency of 54.4% of TOC removal was achieved within 60 min of degradation (removal of 6.22 mg/L of TOC using 3.125 mM/L of H_2O_2). It was also observed that the oxidation reaction was more efficient in the initial 5 min of reaction, when a higher TOC decay occurred. From Fig. 1A, it is possible to estimate that in 1 h each 1 mM/L of H_2O_2 makes it possible to oxidize 2.17 mg/L of TOC. Based on this finding, in the kinetics experiments using a 1.05 mg/L PFF, the H_2O_2 dosages used were 0.50 (dosage sufficient to oxidize 100% TOC in 60 min) and 0.25 mM/L.

3.2. Definitive degradation studies

A second degradation study was performed on different ECs (Supplementary Table S2) using the PFF concentration as a reference for the kinetic study. According to Table 1, the pH of the reaction medium had a greater influence on PFF degradation than the concentration of H_2O_2. This occurred not only because pH alters the dissociation balance of H_2O_2, but also because pH influences the degradation mechanisms of PFF in the presence of $HO^{\bullet}$ radicals.

The degradation test in the presence of H_2O_2 revealed the influence of UV radiation on the PFF degradation, which resulted in a low oxidation rate and a single kinetic step. This degradation process provided by UV-C radiation is associated with the breaking-up of chemical bonds with lower bond enthalpy.

The UV-pH-H_2O_2 trio provided a remarkable increase in the degradation of the PFF molecule (ECs 3–6). Two profiles in the PFF concentration decay were observed: the first one was a faster step up to 5 min; and the second was a slower step from 5 up to 60 min. The overall degradation of the PFF molecule was more effective in an alkaline medium (ECs 4 and 6) than in an acidic medium (ECs 3 and 5), which revealed the direct influence of the acid–base equilibrium of H_2O_2 molecule.

The faster step may be associated with the high rate generation of $HO^{\bullet}$ radicals from H_2O_2 (Reaction 1), followed by dissociation of the weaker bonds. The slower step may be associated with the decay in the concentration of $HO^{\bullet}$ radicals and consequent increase in the concentration of the by-products that provoked the secondary reactions. This finding corroborates the study by Mishchuk et al. [26], which showed that H_2O_2 dissociation kinetics initially occurs in a fast step, followed by a step with a lower kinetic rate. The oxidation of organic carbon in two kinetic steps (an initial fast and a second slow) was also evidenced in another study that involved the degradation of indigo dye by H_2O_2/UV-C [27].

Fig. 1B indicates that at the very beginning of degradation of the PFF molecule, the acidic medium (ECs 3 and 5) was more effective (degradation rate of 82.0% for EC 5 and 62.8% for EC 3) than the alkaline medium (degradation of 18.5% EC 6 and 19.3% for EC 4). At the slow step,

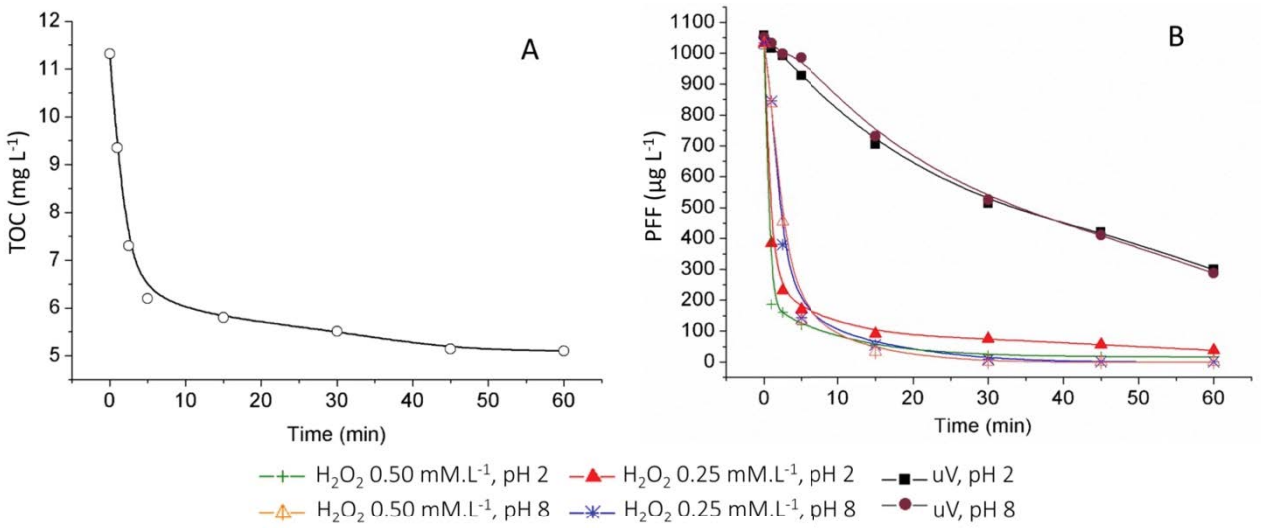

Fig. 1. TOC decrease for a 50 mg/L PFF solution under EC 3 and profiles of decay of the concentration of PFF under six different ECs.

Table 1
Degradation of PFF according to each experimental condition and ANOVA

Time (min)	PFF degradation rate (%)					
	EC 1: UV-pH 2	EC 2: UV-pH 8	EC 3: UV-pH 2 H_2O_2 0.25 mM/L	EC 4: UV-pH 8 H_2O_2 0. 50 mM/L	EC 5: UV-pH 2 H_2O_2 0.25 mM/L	EC 6: UV-pH 8 H_2O_2 0.50 mM/L
0–1	2.09	0.39	62.87	18.50	82.03	19.31
2–2.5	4.29	3.76	77.69	63.29	84.50	56.14
2.5–5	10.54	4.96	83.60	86.22	88.47	87.01
5–15	32.04	29.51	91.27	94.74	95.50	96.88
15–30	50.51	49.33	92.83	99.19	97.92	100.00
30–45	59.39	60.37	94.60	100.00	98.29	100.00
45–60	71.18	72.23	96.42	100.00	98.46	100.00

ANOVA

Factor	SS	MS	*F*	*p*
(1) H_2O_2 (mM/L)	455.4	455.4	3,816.6	0.000
(2) pH	1,009.3	1,009.3	8,458.8	0.000
1 by 2	84.2	84.2	705.9	0.000
Error	0.48	0.12		

however, the reactions conducted in the alkaline medium yielded higher degradation rates than the acidic medium. In the test conducted in EC 6, 100% degradation was completed in 30 min. Despite the complete disappearance of PFF at 30 min, the TOC decay data under a proportionally similar oxidation condition suggests that the molecule was not completely mineralized.

Crittenden et al. [25] and Azizi et al. [28] have reported that under an alkaline medium, hydrogen peroxide is deprotonated according to Reaction 2. The HO_2^- ion reacts with an un-dissociated H_2O_2 molecule according to Reaction 3, leading to the formation of molecular oxygen and water, instead of $HO^\bullet$ radicals under UV-C radiation as happened in Reaction 1.The HO_2^- ion is one of the largest hydroxyl radical scavengers (Reaction 4) whose reaction rate with hydroxyl radicals is twice as fast as hydrogen peroxide [25]. For these reasons, the degradation rate of the PFF was higher in the acidic medium in the first minute of reaction.

$$H_2O_2 + \text{UV-C} \rightarrow 2HO^\bullet \quad (1)$$

$$H_2O_2 + HO^- \rightarrow HO_2^- + H_2O \quad (2)$$

$$HO_2^- + H_2O_2 \rightarrow H_2O + O_2 + HO^- \quad (3)$$

$$OH^\bullet + HOO^- \rightarrow HOO^\bullet + HO^- \quad (4)$$

The variation of pH during the reaction time is shown in Fig. 2A. In reactions carried out under alkaline medium and with the presence of H_2O_2, the progressive decay of pH indicates that the HO^- ions were consumed along with the reactions. Since these reactions provided the highest degradation rates, this suggests that HO^- ions were present, directly or indirectly, in the degradation of PFF and its by-products. Moreover, some authors Hermes et al. [20] and Lay [29] have observed that during reactions with H_2O_2/UV-C in the alkaline medium the pH decay can also be associated with the production of mineral acids or carbon dioxide or acid intermediates. In the degradation s only with UV-C alone, there was no significant variation in pH.

In the acidic medium, the pathway described by Reaction 4 is more favorable for two reasons: first, the generation of HO^- ions compensates the ionic equilibrium of the reactional medium; second, there are oxidation reactions by electron abstraction that generate organic ions or halogens ions (Cl^- and Br^-) from PFF molecule.

This has been observed in experiments with H_2O_2/UV-C [30] for remediation of biodiesel effluents: as the pH decreases, smaller doses of H_2O_2 were required. This observation was justified by the presence of H_2SO_4, used in the acidification step, which tends to promote parallel reactions, affecting the efficiency of the H_2O_2 consumption, as Soares et al. [31] also found, that H^+ and HSO_4^- ions tend to act as hydroxyl radical scavengers according to Reactions 5, 6, and 7. These hypotheses can be confirmed by variations in H^+ and HSO_4^- concentrations, calculated from the pH of the reaction medium. For both doses, 0.25 and 0.5 mM/L of H_2O_2, the initial concentration of these ions was 8.3 mM/L at pH 2. After 30 min of reaction, the concentration of H^+ and HSO_4^- ions dropped to 1.25 mM/L with 0.25 mM/L H_2O_2. For 0.50 mM/L H_2O_2, the final concentration of H^+ and HSO_4^- was 0.53 mM/L.

$$HSO_4^- + OH^\bullet \rightarrow SO_4^{\bullet -} + H_2O \quad (5)$$

$$H_2O_2 + H^+ \rightarrow H_3O_2^+ \quad (6)$$

$$OH^\bullet + H^+ + e^- \rightarrow H_2O \quad (7)$$

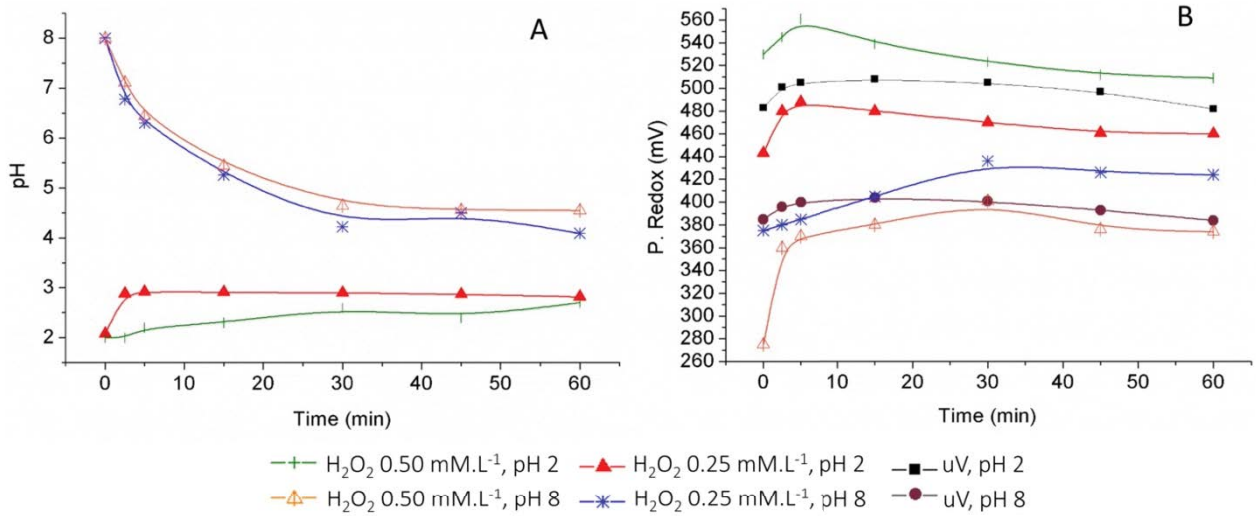

Fig. 2. pH variation over time of ECs 3–6 and redox potential variation over time of different ECs.

Fig. 2B shows the redox potential values monitored over time for each oxidation condition. The reactions in the acidic medium had a predominantly higher redox potential than the reactions in the alkaline medium. This happens because the concentration of some species involved in the degradation process is drastically altered with a pH change. Consequently, a change is provided in the terms governing the law of mass action, as indicated by Nernst's equation

Reactions carried out in the acidic medium reached the maximum redox potential at 5 min, followed by a sharp decay; reactions in the alkaline medium reached the maximum redox potential at 30 min of oxidation. This observation is in agreement with PFF degradation curves, where the reactions conducted in the acidic medium were more efficient in the initial stage of oxidation (fast step, first five minutes), while the reactions in alkaline medium promoted significant degradation in the two steps (from initial to near 60 min).

These facts indicate that changes in the redox potential over time may be associated with the formation of species involved in the H_2O_2 photolysis reaction, such as HOO^- and $HOO^\bullet$. The redox potential of the $HO^\bullet$ radical is considered high when compared to other species (E_0 = 2.73 V vs. NHE) [32]; this influence over the redox potential of the reaction medium is significantly higher than other species.

At pH 2.0, the higher dosage of H_2O_2 (0.50 mM/L) yielded higher redox potential value than the lower (0.25 mM/L), but at pH 8 the opposite was observed. Thus, in the acidic medium, the increase in $HO^\bullet$ concentration can be directly related to the increase of the H_2O_2 concentration, as already observed by some authors Li et al. [33] and Luo et al. [34]. They also observed that there is a maximum limit and that, after a certain concentration, the reaction yield is decreased.

After 60 min of photo-assisted oxidation, the residual H_2O_2 analyses were carried out; in all experiments (ECs 3–6) the resulting concentration was below the limit of the detection of the method (2.7 mg/L or 0.08 mM/L) Thus, with an initial dosage of 0.50 mM/L H_2O_2, about 97% of this reagent was consumed; similarly, for the initial dosage of 0.25 mM/L, more than 97% was consumed.

3.3. Kinetic study

In this first kinetic evaluation step, both the first-order and second-order models were fitted to the data from the 0–60 min oxidation process. Kinetic constant (k) and correlation coefficient (r) for the fitted models are shown in Table 2. By considering the quality of the fitted models, the pseudo-second-order model was better for pH variations under H_2O_2 25.0 mM/L; while the pseudo-first-order model was better for pH variations under H_2O_2 50.0 mM/L. Although both models were suitable, the pseudo-first-order model was chosen for the kinetic evaluation, since it has been more widely reported for different oxidative processes in the degradation of pesticides [10,11,28,30].

Regarding the influence of pH under the UV-H_2O_2 25 mM/L conditions (ECs 3–4), the variation of pH from 2.0 to 8.0 increased the kinetic constant of PFF degradation by 3.73 times (25.7/6.9 s^{-1}), while under the UV-H_2O_2 50 mM/L conditions (ECs 5–6), the kinetic constant of PFF degradation increased 4.22 times (38.2/9.05 s^{-1}).

These findings indicate that an increase in H_2O_2 concentration increases the effect of pH over the $HO^\bullet$ formation. As already explained, the excess H_2O_2 in the fast step is not favorable for $HO^\bullet$ formation. However, as H_2O_2 is consumed and the slow step starts, the excess of H_2O_2 allows an affective formation of $HO^\bullet$ which is more influenced by pH. These facts are illustrated in the degradation curves (Fig. 1B), where the slow step for reactions conducted in the alkaline medium was more effective than in the acidic medium. This information also corroborates the redox potential data, directly related to the formation of HO radicals. This excess of H_2O_2 is characterized by the presence of reagent that has not been converted into $HO^\bullet$ radicals. With the redox potential data, at pH 2 the excess of H_2O_2 was completely converted into $HO^\bullet$ radicals until the end of the first 5 min of reaction. In the basic medium, this excess

of H_2O_2 was present up to 30 min of oxidation. The termination of the conversion of H_2O_2 to $HO^•$ radicals is indicated by the decay of the redox potential levels of the reaction medium. This consumption of H_2O_2 was verified after 60 min of reaction by a direct analysis of this reagent.

Regarding the influence of the increase in the H_2O_2 concentration under acidic medium (ECs 3–5), the variation of H_2O_2 concentration from 25.0 to 50.0 mM/L increased the kinetic constant of PFF degradation by 1.31 times (9.05/6.9 s^{-1}); while under the alkaline medium (ECs 4–6), the kinetic constant of PFF degradation increased by 1.48 times (38.2/25.7 s^{-1}). Two authors Azizi et al. [28] and Costa et al. [30] have concluded that for the photo-assisted oxidation, the kinetic constant can be described as a function of H_2O_2 concentration and pH.

The variation of pH in the direct photolysis in the UV-C (ECs 1–2) did not present significant influence over the kinetic constant for the photo-assisted oxidation. This indicates that the pH influence on the oxidation of the PFF molecule may be related only to the ionic equilibrium of the H_2O_2. The ionic species involved photolysis reaction (HO^-, H^+ and HOO^-) may be directly or not at all involved in the decomposition or reaction of H_2O_2 and $HO^•$ formation, as described in the following equations.

$$H_2O_2 \leftrightarrow HOO^- + H^+ \quad (8)$$

$$HO^• + HOO^- \rightarrow HOO^• + HO^- \quad (9)$$

Given that the oxidation of the PFF molecule occurred in two steps, a first fast and a second slow, the decay of TOC and concentration of PFF were evaluated based on the fit of the pseudo-first-order model for each step (Fig. 3A and B). In both cases, oxidation was carried out at pH 8 and 0.25 mM/L of H_2O_2 was used for each 1 mg/L of PFF, as previously described in section 2.4. In terms of TOC decay, the kinetic constant of the fast step was 30 times higher than the slow step (2.010^{-3} s^{-1}/6.010^{-5} s^{-1}) while in terms of PFF concentration, it was 3.58 times (6.8×10^{-3} s^{-1}/1.9×10^{-3} s^{-1}).

In terms of TOC, the decay in the slow step is related to the oxidation of molecular structures more resistant to oxidation, since the structures most susceptible to oxidation are quickly converted into CO_2 and H_2O. In terms of PFF concentration, the decay in the slow step is related to the presence of by-products that start competitive reactions. These observations explain the differences between the kinetic constant in both steps.

Table 2
Values of kinetic constant and coefficient of determination for pseudo-first-order and pseudo-second-order models

EC	Fitted model			
	Pseudo-first-order		Pseudo-second-order	
	k (s^{-1}) × 10^{-4}	R^2	k (L/μg·s) × 10^{-6}	R^2
EC 1: UV-pH 2	3.61	0.99	0.66	0.99
EC 2: UV-pH 8	4.46	0.99	0.66	0.99
EC 3: UV-pH 2 H_2O_2 0.25 mM/L	6.90	0.86	6.60	0.98
EC 4: UV-pH 8 H_2O_2 0. 50 mM/L	25.7	0.96	20.0	1.00
EC 5: UV-pH 2 H_2O_2 0.25 mM/L	9.05	0.86	18.3	0.98
EC 6: UV-pH 8 H_2O_2 0.50 mM/L	38.2	0.96	35.0	0.99
	Average R^2		Average R^2	

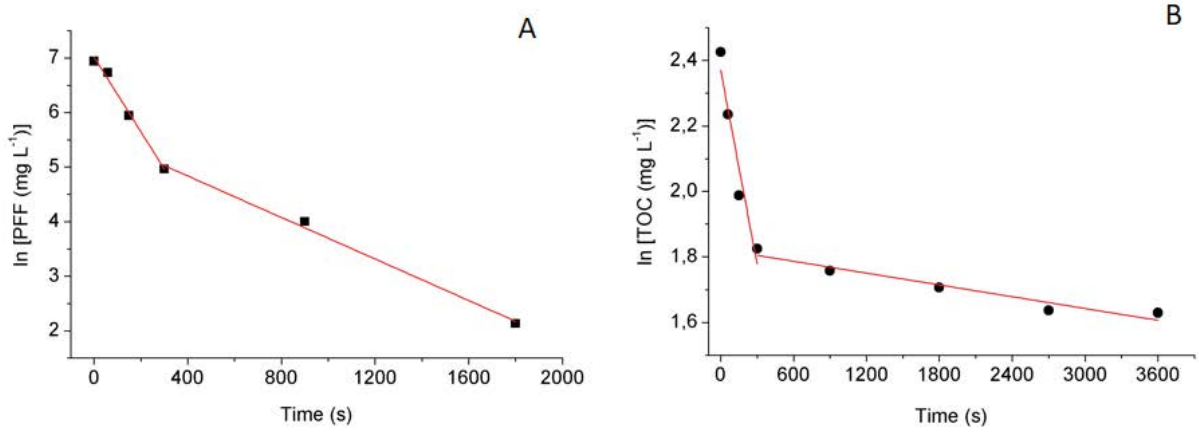

Fig. 3. Fit of experimental data to the pseudo-first-order for degradation of PFF molecule by EC 6 in terms of TOC (A) PFF 50 mg/L and (B) PFF concentration PFF 1 mg/L.

It is worth mentioning that the monitored analytical signal (abundance of a given *m*/*z* ratio) is affected by any modification in the PFF structure. Therefore, for example, decreases in the concentration of this pollutant may be associated with the loss of a single carbon.

3.4. Analysis of by-products and degradation pathway proposal

The degradation products (by-products) of the PFF molecule can be identified by the results from mass spectrometry measurements in the ESI$^+$ mode. For this, a PFF solution before and after photo-assisted oxidation (EC 6) was analyzed; the results are in Supplementary Fig. S2A and B, respectively. The ions observed in this mode are quasi-molecular ions generated by the addition of H^+ (denoted by $[M + H]^+$) or Na^+ (denoted by $[M + Na]^+$) ion. In this work, the ions observed were of the $[M + H]^+$ type and denoted by observed *m*/*z* (Obs. *m*/*z*) while the original *m*/*z* ratios were denoted by corrected *m*/*z* (Corr. *m*/*z*).

Given the large number of peaks in the mass spectra of PFF and aiming at the identification of by-products, the only peaks considered were those with relative abundance higher than 10 (peaks 377, 375, 173 and 155 in Fig. S2A, and peaks 371, 257, 173, 155, 149, 111 and 84 in Fig. S2B. In addition, a molecular map of PFF binding dissociation enthalpy was developed to target the degradation pathways. The result is shown in Fig. S3.The computational tool used was ALFABET [35], which uses a trained graphical neural network to determine enthalpy values.

Regarding Fig. S2A peaks 375 and 377 (isotope effect) correspond to the molecular ion of the PFF molecule. Peaks 173 and 155 were both present before and after the photo-assisted peroxidation, indicating that both are obtained regardless of the presence of H_2O_2. The oxidation of PFF was initiated according to Pathway 1, Fig. 4, with the absorption of radiant energy by the O–P bond, promoting a homolytic scission, yielding the radicals IP-1 and IP-2. The energy for this scission was provided by the irradiation from a mercury vapor lamp at 254 nm [36], in studies on spectra of UV-C absorption of pesticides, found that the PFF molecule has a strong absorption band between 254 nm (ε = 460 ± 30 L/mol·cm) and 285 nm (ε = 380 ± 30 L/mol·cm). According to the estimate of nuclear magnetic resonance (NMR) ^{13}C and ^{1}H for the PFF molecule, presented in Supplementary Fig. S4 and B, the molecular regions of greater electronic shielding are the O–C_2H_5 and S–C_3H_7 branches; thus, this molecular region is more susceptible to an attack of $HO^\bullet$ radicals. Besides, the carbons of these branches have less

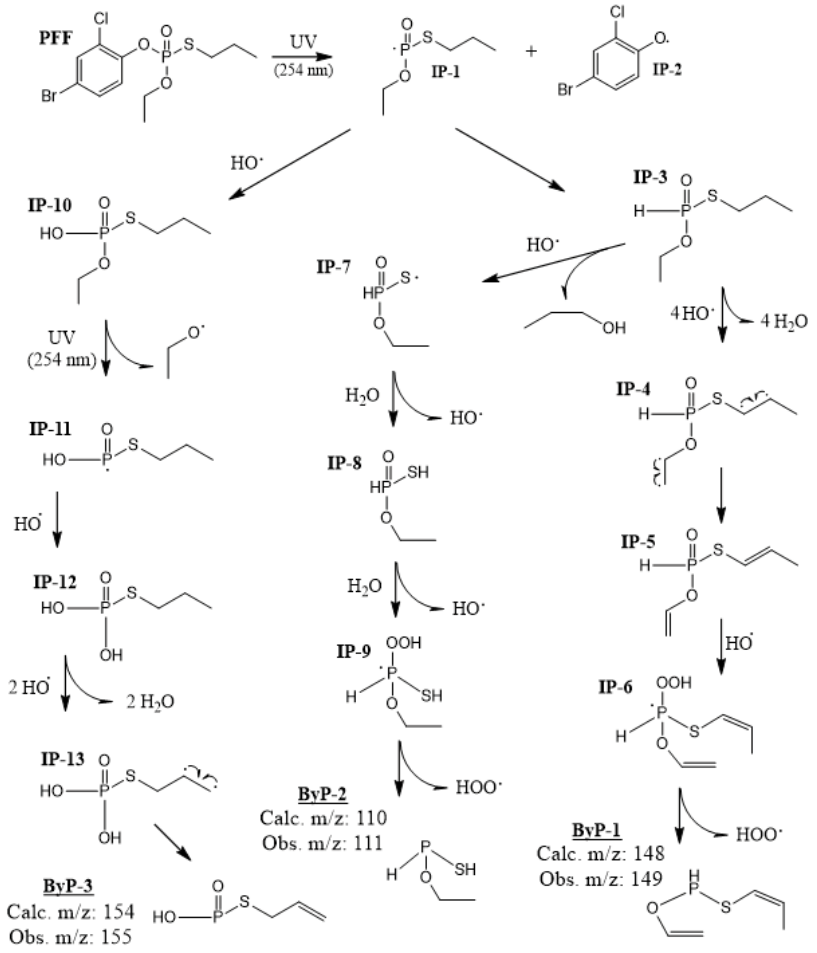

Fig. 4. Pathway 1: formation of *O*-ethenyl-*S*-prop-2-en-1-yl phosphonothioite, *O*-ethyl hydrogen phosphonothioite, and *S*-prop-2-en-1-yl dihydrogen phosphorothioate, respectively.

enthalpy of binding (<89.7 Kcal/mol) than those in other regions of the molecule, as in the benzene aromatic ring (single bond and double bond together >273 Kcal/mol). These observations suggest that the rapid kinetic decay in the first 5 min is associated with the mineralization of branches O–C_2H_5 and S–C_3H_7 present in IP-1.

Thus, the oxidation of PFF was initiated as described in Fig. 4, with the extraction of hydrogen radicals from the water molecules of the reaction medium by IP-1 yielding IP-3 and HO• radical. This same process of water hydrogen extraction has been described by some authors under different oxidation processes [11,37]. The second step, as shown in the figure, is the abstraction of two hydrogen radicals from each alkyl group of IP-3 yielding IP-4 and four water molecules. In the third step, two unsaturations are formed in IP-4, yielding IP-5. The fourth step is the reaction between IP-5 and HO• radical, yielding IP-6. The fifth step is the loss of HOO radical of the structure of IP-6 yielding ByP-10 (*O*-ethenyl-*S*-prop-2-en-1-yl phosphonothioite).

The sixth step start with the reaction between the HO• radical and IP-3, yielding 1-propanol, and IP-7, which were then mineralized into CO_2 and H_2O. The seventh step is the abstraction of the hydrogen radical from water molecules of the reaction medium by IP-7, yielding IP-8, and a HO• radical. The eighth step is the reaction between IP-8 and the HO• radical, yielding IP-9. The ninth step is the loss of four HOO radicals from the structure of IP-9 yielding ByP-11 (*O*-ethyl hydrogen phosphonothioite).

As the HO• radical is generated, the tenth step starts by reacting with IP-1, yielding IP-10. The eleventh step starts with a second absorption of radiant energy by an O–P bond of IP-10, promoting another mineralization of CO_2 and H_2O. The twelfth step was the abstraction of HO• radical from water molecules of the reaction medium by IP-11 yielding IP-12 and the H radical. The thirteenth step is the abstraction of hydrogen radicals from the alkyl group of IP-12 yielding IP-13 and two water molecules. In IP-13, two unsaturations are formed, yielding ByP-9 (*S*-prop-2-en-1-yl dihydrogen phosphorothioate).

As previously described, in addition to having a lower electronic density, which slows down the action of HO• radicals, the IP-2 intermediate has a high bonding intensity, caused by aromaticity and double bonds (binding enthalpy 152 Kcal/mol). Routes for IP-2 mineralization as well involve a greater amount of HO• radicals, described below, indicating that pathways 2, 3 and 4 were possibly the reactions of the slow reaction step. After the homolytic fission of the PFF molecule, IP-2 also extracted the hydrogen radical from water molecules of the reaction medium, yielding IP-13. Pathway 2 (Fig. 5) is started by the dechlorination of IP-13 by HO• radical yielding HClO and IP-14. The second step is the abstraction of the hydrogen radical from water molecules from the reaction medium by IP-14 yielding ByP-4 (4-bromophenol) and HO• radical.

The third step starts with the debromination of ByP-4 by HO• radical yielding HBrO and IP-15. The fourth step is the abstraction of hydrogen radical from water molecules of the reaction medium by IP-15, yielding IP-16, and the HO• radical. The fifth step is the abstraction of HO• radical from IP-16 by another HO• radical from the reaction medium, yielding IP-17, and H_2O_2. The sixth step is the abstraction of hydrogen radical from water molecules of the reaction medium by IP-17, yielding IP-18, and HO• radical. The seventh step is a reaction between IP-18 and six HO• radicals yielding IP-19. The eighth step is reaction IP-19 and six more HO• radicals, yielding IP-20 and

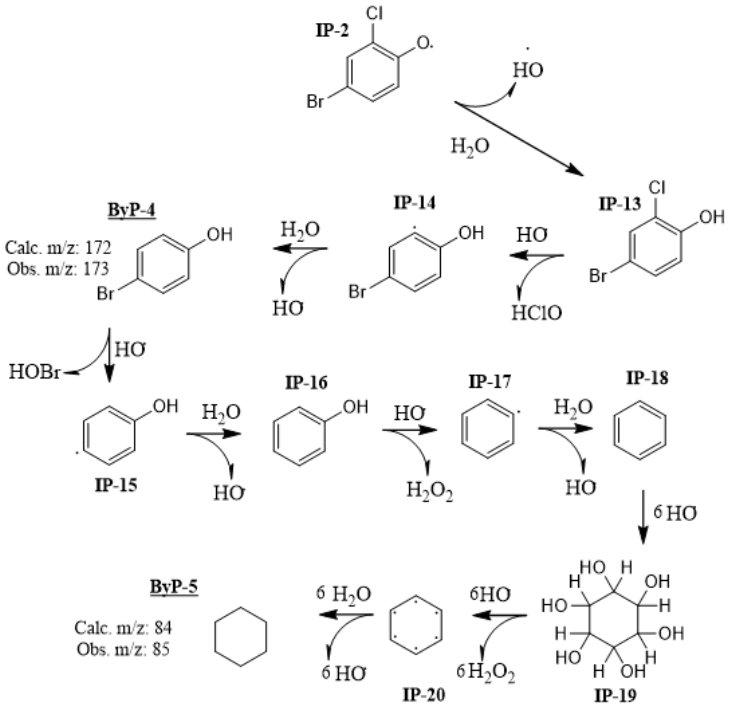

Fig. 5. Pathway 1: formation of the 4-bromophenol and cyclohexane, respectively.

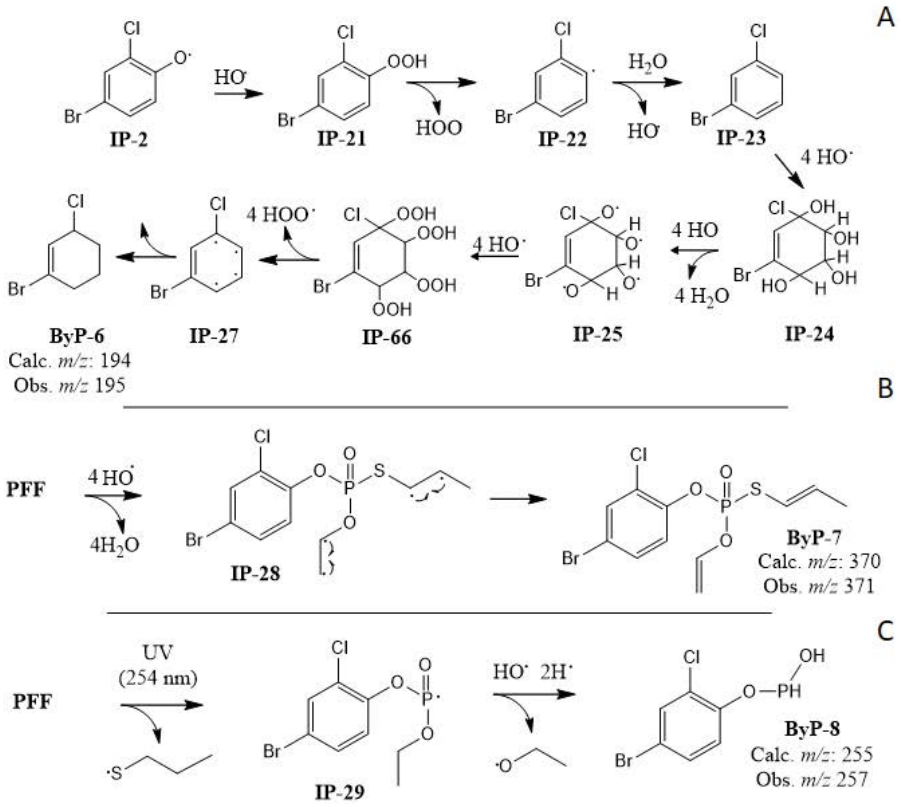

Fig. 6. Pathway 3–5: A-Pathway 3: formation of 1-bromo-3-chlorocyclohex-1-ene, B-Pathway 4: formation of *O*-4-bromo-2-chlorophen yl-*O*-ethyl-*S*-prop-3-enyl, and C-Pathway 5: formation of 4-bromo-2-chlorophenyl hydrogen phosphonate.

H_2O_2. The ninth step is the abstraction of 6 hydrogen radicals from six water molecules of the reaction medium by IP-20, yielding six HO• radicals and ByP-5 (cyclohexane). Then, cyclohexane is mineralized in CO_2 and H_2O.

Pathway 3, shown in Fig. 6A, starts with the reaction between IP-2 and HO• radical yielding IP-21. The second step is the loss of HOO radical in IP-21, yielding IP-22. The third step is the abstraction of hydrogen radical from water molecules of the reaction medium by IP-22 yielding IP-23 and HO• radical. The fourth step is the attack of four HO• radicals in two pi bonds of IP-23, yielding IP-24. The fifth step is the abstraction of four hydrogen radicals from the four OH groups of IP-24, yielding IP-25. The sixth step is the reaction between IP-25 and four HO• radicals yielding IP-26. The seventh step is the loss of four HOO• radicals of the structure of IP-26 yielding IP-27. The eighth step is the abstraction of four hydrogen radicals from four water molecules of the reaction medium by IP-27 yielding four HO• radicals and ByP-6. It is worth mentioning that IP 27 and ByP-6 can present six different structures obtained by the resonance of pi electrons and radicals. Definitive identification of which isomer(s) is(are) formed could be made through NMR of ^{1}H and ^{13}C. Unfortunately, this feature was not available in our research context.

Pathways 4 and 5 are shown in Fig. 6B and C. Pathway 4 starts with the abstraction of two hydrogen radicals from each alkyl group of the PFF molecule yielding IP-28 and four water molecules. This reaction is favored by the high electronic density in this molecular region, as previously discussed. In IP-28 two unsaturations are formed, yielding ByP-7 (*O*-4-bromo-2-chlorophenyl-*O*-ethyl-*S*-prop-3-enyl). Pathway 5 starts with the absorption of radiant energy by the S–P bond, promoting a homolytic scission in the PFF molecule, yielding the intermediate radicals IP-29 and Thiyl. The second step starts with the absorption of radiant energy by the O–P bond, promoting another homolytic scission, yielding ethoxy radical and ByP-8 (4-bromo-2-chlorophenyl hydrogen phosphonite). Supplementary Table S3 contains the IUPAC names, the *m*/*z* ratios, and the chemical formulas of all identified by-products.

4. Conclusion

The evaluation of the kinetic models indicated that the pseudo-first-order model was able to describe the kinetic behavior of the oxidation reactions of PFF by the H_2O_2/UV-C process under an alkaline medium. Kinetic data indicated that PFF degradation occurred in two steps: a fast one (0–5 min) and a slow (5–60 min). Reactions conducted in the alkaline medium promoted significant oxidation in both steps while in the acidic, only in the fast step. The measurements of redox potential indicated that this behavior is due to the differences in the efficiency of hydroxyl radical in both media, which determined the equilibrium in aqueous medium of H_2O_2.

Significant differences between the kinetic behavior for degradation of TOC ($k = 2.0 \times 10^{-3}$ s^{-1} fast step, $k = 6.0 \times 10^{-5}$ s^{-1} slow step) and PFF ($k = 6.8 \times 10^{-3}$ s^{-1} fast step, $k = 1.9 \times 10^{-3}$ s^{-1}

slow step) were observed. These differences showed that the oxidation of organic matter, composed of PFF and its by-products, was slower than the decay of PFF molecule concentration, and as the hydroxyl radicals start to oxidize the by-products that had been generated, the degradation rate of PFF decreased.

This study indicated that the rapid oxidation step is related to the mining of the O–C_2H_5 and S–C_3H_7 chains of the intermediate *O*-ethyl *S*-propyl phosphonothioate. This occurs because these molecular regions have higher electron density and lower binding energies. The slow oxidation stage comprises the 4-bromo-2-chlorophenyl mineralization and derivatives. This detailed study of the degradation pathways made it possible to identify 8 oxidation by-products and 29 reaction intermediates. In the oxidation routes, the main mechanisms involved in the mineralization of PFF by the action of $OH^{\bullet}$ radicals and UV-C were electron abstraction reactions, OH abstraction, $H^{\bullet}$ abstraction, substitution, electron displacement, and addition. The detailed description of the PFF degradation pathway and presentation of reaction mechanisms improves the knowledge of the oxidation mechanisms mediated by $OH^{\bullet}$, facilitating the understanding of the degradation of organic pollutants in general.

Acknowledgments

The authors wish to thank Fundação de Apoio à Pesquisa do Estado da Paraíba (FAPESQ), Conselho Nacional de Desenvolvimento Científico e Tecnológico (CNPq), Coordenação de Aperfeiçoamento de Pessoal Nível Superior (CAPES) and Financiadora de Estudos e Projetos (FINEP) for financial support.

References

[1] M.A. González-Curbelo, B. Socas-Rodríguez, M. Herrero, A.V. Herrera-Herrera, J. Hernández-Borges, Dissipation kinetics of organophosphorus pesticides in milled toasted maize and wheat flour (gofio) during storage, Food Chem., 229 (2017) 854–859.

[2] W.-J. Li, Y. Li, D. Ning, Q. Liu, L. Chang, W.-J. Ruan, An Fe(II) metal–organic framework as a visible responsive photo-Fenton catalyst for the degradation of organophosphates, New J. Chem., 42 (2018) 29–33.

[3] R. Pamanji, B. Yashwanth, M.S. Bethu, S. Leelavathi, K. Ravinder, J. Venkateswara Rao, Toxicity effects of profenofos on embryonic and larval development of Zebrafish (*Danio rerio*), Environ. Toxicol. Pharmacol., 39 (2015) 887–897.

[4] P.V. Toan, Z. Sebesvari, M. Bläsing, I. Rosendahl, F.G. Renaud, Pesticide management and their residues in sediments and surface and drinking water in the Mekong Delta, Vietnam, Sci. Total Environ., 452–453 (2013) 28–39.

[5] X.T. Lu, C. Yu, Enantiomer-specific profenofos-induced cytotoxicity and DNA damage mediated by oxidative stress in rat adrenal pheochromocytoma (PC_{12}) cells, J. Appl. Toxicol., 34 (2014) 166–175.

[6] R.O. Sule, L. Condon, A.V. Gomes, A common feature of pesticides: oxidative stress-the role of oxidative stress in pesticide-induced toxicity, Oxid. Med. Cell. Longevity, 2022 (2022) 5563759, doi: 10.1155/2022/5563759.

[7] A.M. Parker, Y. Lester, E.K. Spangler, U. von Gunten, K.G. Linden, UV/H_2O_2 advanced oxidation for abatement of organophosphorous pesticides and the effects on various toxicity screening assays, Chemosphere, 182 (2017) 477–482.

[8] X. Li, D. Zhang, Z. Liu, Y. Xu, D. Wang, Synthesis, characterization of a ternary Cu(II) Schiff base complex with degradation activity of organophosphorus pesticides, Inorg. Chim. Acta, 471 (2018) 280–289.

[9] C. Zamy, P. Mazellier, B. Legube, Phototransformation of selected organophosphorus pesticides in dilute aqueous solutions, Water Res., 38 (2004) 2305–2314.

[10] C. Fang, X. Zhang, X. Lou, Y. Shi, Y. Tang, D. Huang, J. Liu, Y. Guo, Insights into effect of chloride ion on the degradation of 4-bromo-2-chlorophenol by sulphate radical-based oxidation process, Int. J. Environ. Anal. Chem., (2022), doi: 10.1080/03067319.2022.2060091.

[11] D. Angthararuk, M. Harir, P. Schmitt-Kopplin, S. Sutthivaiyakit, A. Kettrup, P. Sutthivaiyakit, Degradation products of profenofos as identified by high-field FTICR mass spectrometry: isotopic fine structure approach, J. Environ. Sci. Health., Part B, 52 (2017) 10–22.

[12] M. Menager, J.S. Pilichowski, M. Sarakha, Reaction pathways for the photodegradation of the organophosphorus cyanophos in aqueous solutions, Photochem. Photobiol., 86 (2010) 247–254.

[13] Y. Chen, Y. Xiong, Z. Wang, Y. Chen, G. Chen, G. Liu, UV/ferrate(VI) oxidation of profenofos: efficiency and mechanism, Desal. Water Treat., 55 (2015) 506–513.

[14] C.P. James, E. Germain, S. Judd, Micropollutant removal by advanced oxidation of microfiltered secondary effluent for water reuse, Sep. Purif. Technol., 127 (2014) 77–83.

[15] F.L. Rosario-Ortiz, E.C. Wert, S.A. Snyder, Evaluation of UV/H_2O_2 treatment for the oxidation of pharmaceuticals in wastewater, Water Res., 44 (2010) 1440–1448.

[16] N.M. Costa, V.M. Silva, G. Damaceno, R.M.F. Sousa, E.M. Richter, A.E.H. Machado, A.G. Trovó, Integrating coagulation-flocculation and UV-C or H_2O_2/UV-C as alternatives for pre- or complete treatment of biodiesel effluents, J. Environ. Manage., 203 (2017) 229–236.

[17] M.M. Amin, B. Jaberian, B. Bina, M. Sadani, R. Hadian, G. Bonyadinejad, M.M.A. Moazzam, 2009. Advanced oxidation of the endosulfan and profenofos in aqueous solution using UV/H_2O_2 process, Environ. Asia, 7 (2014) 57–64.

[18] M.I. Badawy, M.Y. Ghaly, T.A. Gad-Allah, Advanced oxidation processes for the removal of organophosphorus pesticides from wastewater, Desalination, 194 (2006) 166–175.

[19] E.N. Evgenidou, I.K. Konstantinou, D.A. Lambropoulou, Occurrence and removal of transformation products of PPCPs and illicit drugs in wastewaters: a review, Sci. Total Environ., 505 (2015) 905–926.

[20] N. Hermes, K.S. Jewell, A. Wick, T.A. Ternes, Quantification of more than 150 micropollutants including transformation products in aqueous samples by liquid chromatography-tandem mass spectrometry using scheduled multiple reaction monitoring, J. Chromatogr. A, 1531 (2018) 64–73.

[21] T. Cáceres, M. Megharaj, R. Naidu, Toxicity of fenamiphos and its metabolites to the cladoceran *Daphnia carinata*: the influence of microbial degradation in natural waters, Chemosphere, 66 (2007) 1264–1269.

[22] S. Benfeito, T. Silva, J. Garrido, P.B. Andrade, M.J. Sottomayor, F. Borges, E. Manuela Garrido, Effects of chlorophenoxy herbicides and their main transformation products on DNA damage and acetylcholinesterase activity, BioMed Res. Int., 2014 (2014) 709036, doi: 10.1155/2014/709036.

[23] C. Matsubara, N. Kawamoto, K. Takamura, Oxo[5, 10, 15, 20-tetra(4-pyridyl)porphyrinato]titanium(IV): an ultra-high sensitivity spectrophotometric reagent for hydrogen peroxide, Analyst, 117 (1992) 1781–1784.

[24] H.T. Madsen, E.G. Søgaard, J. Muff, Study of degradation intermediates formed during electrochemical oxidation of pesticide residue 2,6-dichlorobenzamide (BAM) in chloride medium at boron doped diamond (BDD) and platinum anodes, Chemosphere, 120 (2015) 756–763.

[25] J.C. Crittenden, S. Hu, D.W. Hand, S.A. Green, A kinetic model for H_2O_2/UV process in a completely mixed batch reactor, Water Res., 33 (1999) 2315–2328.

[26] N.A. Mishchuk, L.L. Lysenko, O.V. Zayats, Investigation of the kinetics of catalytic decomposition of hydrogen peroxide

depending on the solution phase state, J. Water Chem. Technol., 31 (2009) 71–80.
[27] R.O. Ramos, M.V.C. Albuquerque, W.S. Lopes, J.T. Sousa, V.D. Leite, Degradation of indigo carmine by photo-Fenton, Fenton, H_2O_2/UV-C and direct UV-C: comparison of pathways, products and kinetics, J. Water Process Eng., 37 (2020) 101535, doi: 10.1016/j.jwpe.2020.101535.
[28] E. Azizi, M. Fazlzadeh, M. Ghayebzadeh, L. Hemati, M. Beikmohammadi, H.R. Ghaffari, K. Sharafi, Application of advanced oxidation process (H_2O_2/UV) for removal of organic materials from pharmaceutical industry effluent, Environ. Prot. Eng., 43 (2017) 183–192.
[29] Y.S. Lay, Oxidation of 1,2-Dibromo-3-chloropropane in Groundwater Using Advanced Oxidation Processes, Ph.D. Dissertation, University of California, Los Angeles, 1989.
[30] N.M. Costa, V.M. Silva, G. Damaceno, R.M.F. Sousa, E.M. Richter, A.E.H. Machado, A.G. Trovó, Integrating coagulation-flocculation and UV-C or H_2O_2/UV-C as alternatives for pre- or complete treatment of biodiesel effluents, J. Environ. Manage., 203 (2017) 229–236.
[31] P.A. Soares, R. Souza, J. Soler, T.F.C.V. Silva, S.M.A. Guelli, U. Souza, R.A.R. Boaventura, V.J.P. Vilar, Remediation of a synthetic textile wastewater from polyester-cotton dyeing combining biological and photochemical oxidation processes, Sep. Purif. Technol., 172 (2017) 450–462.
[32] P. Avetta, A. Pensato, M. Minella, M. Malandrino, V. Maurino, C. Minero, K. Hanna, D. Vione, Activation of persulfate by irradiated magnetite implications for the degradation of phenol under heterogeneous photo-Fenton-like conditions, Environ. Sci. Technol., 49 (2015) 1043–1050.
[33] Q. Li, N. Gao, Y. Deng, X. Ma, W. Chu, Factors affecting UV/H_2O_2 oxidation of 17α-ethynyestradiol in water. Clean–Soil, Air, Water, 41 (2013) 143–147.
[34] C. Luo, J. Ma, J. Jiang, Y. Liu, Y. Song, Y. Yang, Y. Guan, D. Wu, Simulation and comparative study on the oxidation kinetics of atrazine by UV/H_2O_2, UV/HSO_5^- and UV/$S_2O_8^{2-}$, Water Res., 80 (2015) 99–108.
[35] P.C. St. John, Y. Guan, Y. Kim, S. Kim, R.S. Paton, Prediction of organic homolytic bond dissociation enthalpies at near chemical accuracy with sub-second computational cost, Nat. Commun., 11 (2020) 2328, doi: 10.1038/s41467-020-16201-z.
[36] C. Zamy, P. Mazellier, B. Legube, Phototransformation of selected organophosphorus pesticides in dilute aqueous solutions, Water Res., 38 (2004) 2305–2314.
[37] M.L. Chacón-Patiño, C. Blanco-Tirado, J.P. Hinestroza, M.Y. Combariza, Biocomposite of nanostructured MnO_2 and fique fibers for efficient dye degradation, Green Chem., 15 (2013) 2920–2928.

Supplementary information

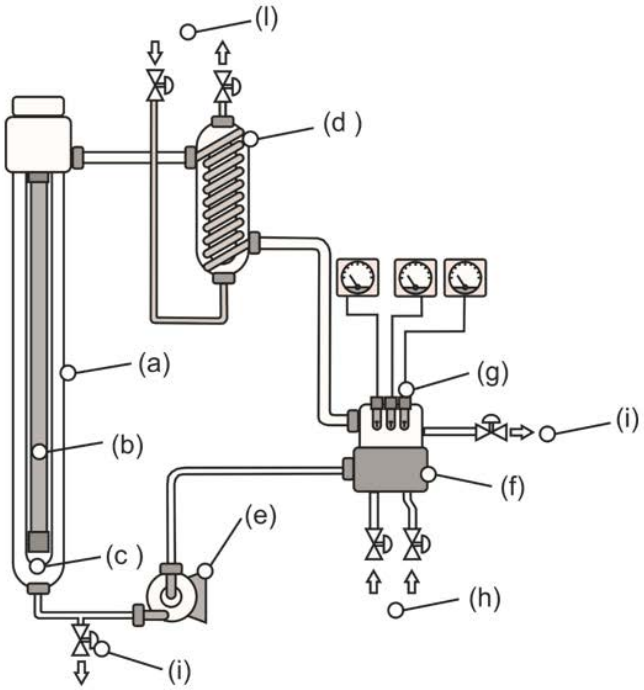

Fig. S1. Configuration of the photocatalytic plug flow reactor: (a) reactor, (b) UV-C lamp, (c) quartz tube, (d) heat exchanger, (e) pump, (f) equalization tank, (g) redox potential (RP), dissolved oxygen (DO) and pH monitors, (h) reagent input and sampling points, (i) drainage tap, and (j) cooling water.

Table S1
Methods and equipment employed in the determination of the parameters/attributes of the processes studied

Parameters/attributes	Method/APHA standard[a]	Equipment employed
pH	Electrometric/4500-H+B	HI2300 pH-Meter; Hanna Instruments, Tamboré, Barueri, SP, Brazil
Dissolved oxygen	Electrometric/4500-O G	ITT 71440 Oximeter Data Logger; ITT Inc., White Plains, NY, USA
Temperature	Electrometric/4500 G	HI-2221 Benchtop Meter; Hanna Instruments
Redox potential	Electrometric/2580	341350A-P Oyster™ Meter; Extech, Nashua, NH, USA
Oxidation products	Direct infusion mass spectrometry (DIMS)	LCQ™ Fleet Ion Trap Mass Spectrometer; Thermo Scientific, Waltham, MA, USA
PFF	UHPLC-MS	UHPLC 3000-LCQ Fleet; Thermo Scientific, Waltham, MA, USA
Total organic carbon	Non-purgeable organic carbon (NPOC)	Multi N/C® 3100 Analyzer with non-dispersive infrared (NDIR) detector; Analytik Jena, Jena, Germany

[a]APHA – Standard Methods for the Examination of Water and Wastewater according to the American Public Health Association.

Table S2
Experimental conditions (EC) for kinetics and by-products studies

EC	Description
1	UV-C radiation at pH 2.0
2	UV-C radiation at pH 8.0
3	UV-C radiation and H_2O_2 25.0 mM/L at pH 2.0
4	UV-C radiation and H_2O_2 25.0 mM/L at pH 8.0
5	UV-C radiation and H_2O_2 50.0 mM/L at pH 2.0
6	UV-C radiation and H_2O_2 50.0 mM/L at pH 8.0

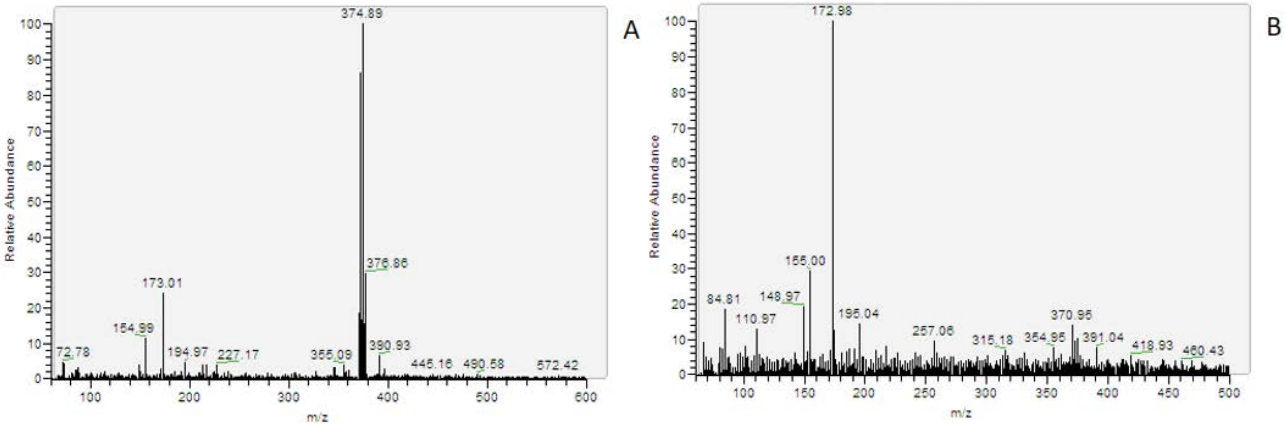

Fig. S2. (a) Mass spectrometer of PFF solution (1,000 μg/L) before photo-assisted oxidation diluted 100 times and (b) mass spectrometer of PFF solution after 60 min of oxidation (EC 6) concentrated 100 times. The dilution and concentration of the solutions were performed during the re-dispersion of the SPME step.

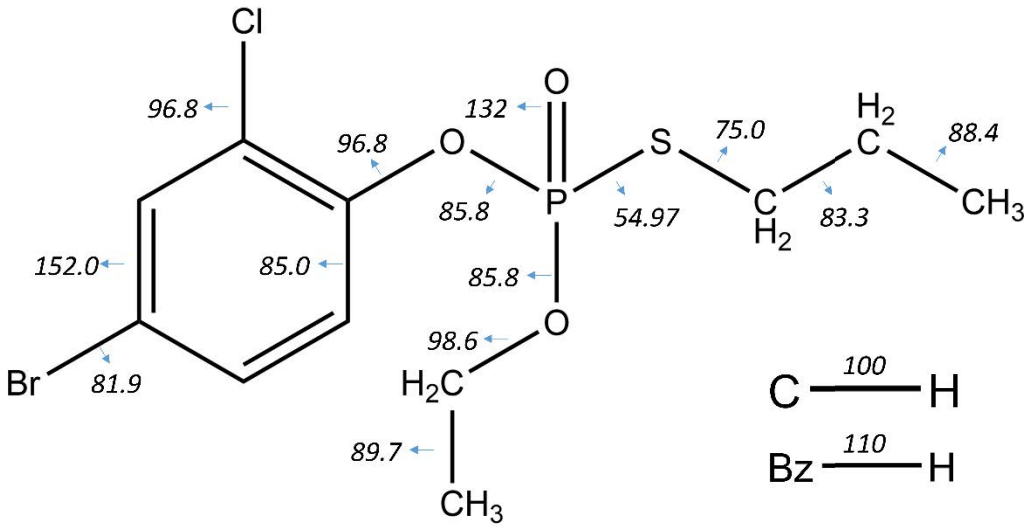

Fig. S3. Molecular map of PFF binding dissociation enthalpy. Values in Kcal/mol.

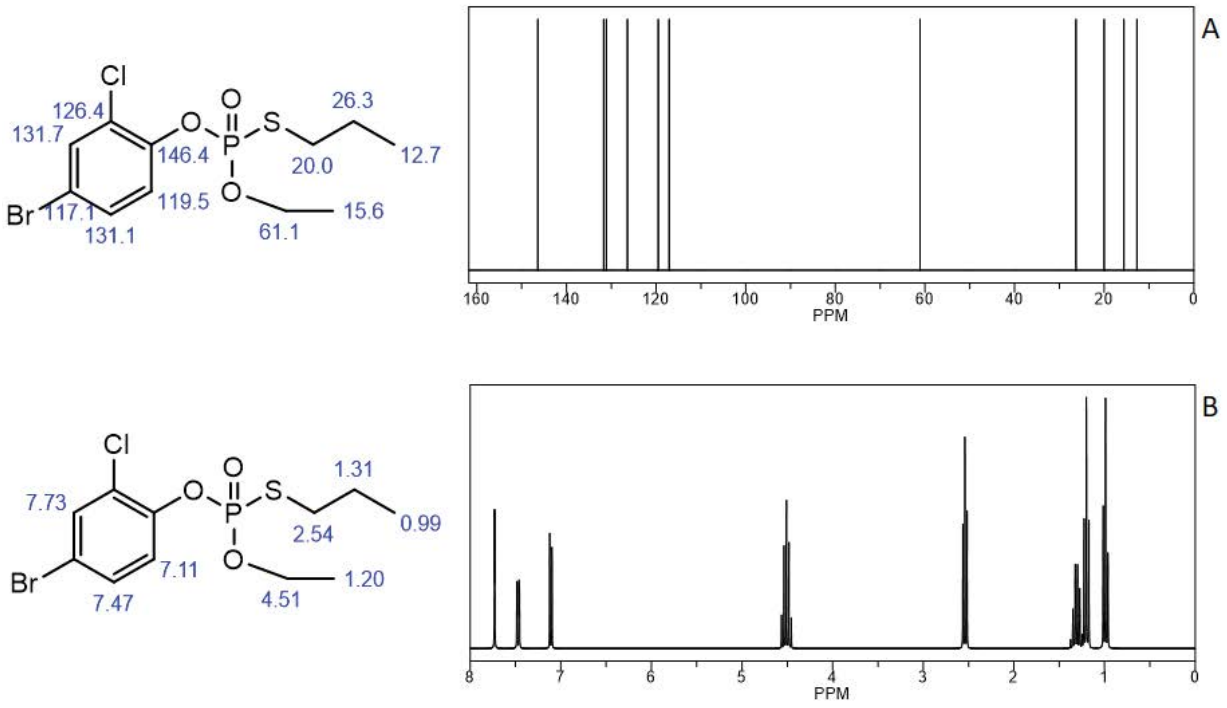

Fig. S4. Simulated NMR spectrum (A) ^{13}C and (B) ^{1}H for the PFF molecule.

Table S3
Identification of the by-products of the PFF molecule

Identifier	Obs. *m/z*	Corr. *m/z*	Chemical formula	IUPAC name
ByP-1	149	148	C_5H_9OPS	*O*-ethenyl *S*-prop-2-en-1-yl phosphonothioite
ByP-2	111	110	C_2H_7OPS	*O*-ethyl hydrogen phosphonothioite
ByP-3	155	154	$C_3H_7O_3PS$	*S*-prop-2-en-1-yl dihydrogen phosphorothioate
ByP-4	173	172	C_6H_5BrO	4-bromophenol
ByP-5	85	84	C_6H_{12}	Cyclohexane
ByP-6	195	194	C_6H_8BrCl	1-bromo-3-chlorocyclohex-1-ene
ByP-7	371	370	$C_{11}H_{12}BrClO_3PS$	*O*-4-bromo-2-chlorophenyl-*O*-ethyl-*S*-prop-3-enyl
ByP-8	257	256	$C_6H_5BrClO_2P$	4-bromo-2-chlorophenyl hydrogen phosphonite